Scott A. Mirowitz, MD

Intracranial Lesion Enhancement with Gadolinium: T1-weighted Spin-Echo versus Three-dimensional Fourier Transform Gradient-Echo MR Imaging[1]

The conspicuity of lesion enhancement with gadopentetate dimeglumine was evaluated subjectively and quantitatively through calculation of contrast-to-noise ratios (C/Ns) on T1-weighted three-dimensional (3D) Fourier transform (FT) gradient-echo (GRE) and two-dimensional (2D) FT spin-echo (SE) images of the brain in 406 consecutive patients. One hundred one enhancing intracranial lesions were present in 61 patients, including intra- ($n = 76$) and extraaxial ($n = 25$) processes of neoplastic ($n = 68$), infectious or inflammatory ($n = 13$), ischemic ($n = 11$), or vascular ($n = 9$) origin. Enhancement was apparent in all lesions on 2DFT SE and 3DFT GRE images, with similar subjective conspicuity in 86.8% (87 of 101) of lesions. Quantitative C/N measurements for 2DFT SE (mean, 17.6) and 3DFT GRE (mean, 17.2) imaging were not significantly different ($P = .72$). These findings, along with the other advantages of 3DFT GRE imaging, indicate that 3DFT GRE examinations are likely to play a major role in the performance of contrast-enhanced MR imaging of the brain.

THREE-DIMENSIONAL (3D) Fourier transform (FT) gradient-echo (GRE) magnetic resonance (MR) imaging offers many important advantages over conventional spin-echo (SE) MR imaging of the brain. These features include improved spatial resolution, demonstration of susceptibility and flow effects for lesion characterization, and ability to retrospectively perform orthogonal or oblique image reconstructions (1,2). Highly T1-weighted GRE images can be acquired with spoiled 3DFT GRE sequences such as fast low-angle shot or spoiled gradient recalled acquisition in the steady state (GRASS; GE Medical Systems, Milwaukee). While unenhanced T1-weighted images may provide useful anatomic information, the use of paramagnetic contrast material allows for marked improvement in the detection and characterization of intracranial lesions (3–6).

Despite the advantages listed above, clinical implementation of 3DFT GRE imaging has been limited, since it has not been demonstrated to provide reliable depiction of pathologic contrast enhancement in patients with intracranial lesions. To my knowledge, there are only a few published reports in which contrast enhancement of intracranial lesions on conventional T1-weighted SE and two-dimensional (2D) or 3D GRE images has been studied, and these reports describe conflicting findings (2,7–9). The objectives of this study were to evaluate the ability of T1-weighted 3DFT GRE imaging to depict contrast enhancement related to intracranial lesions and to compare the conspicuity of such enhancement with that present on conventional T1-weighted SE images.

MATERIALS AND METHODS

Four hundred six consecutive patients who presented for contrast material–enhanced cranial MR imaging between April and December 1991 were studied in this protocol. Patients presenting themselves for pituitary studies and those who could not undergo extended imaging due to severe claustrophobia or discomfort were excluded. MR imaging was performed with a 1.5-T unit (Signa; GE Medical Systems) and a circularly polarized head coil. After performance of an initial sagittal T1-weighted sequence, transaxial spin-density and T2-weighted 3,000/30, 80 (repetition time [TR] msec/echo time [TE] msec) images were acquired with one average, and T1-weighted 500/11 SE images were acquired with two signals averaged. Gadopentetate dimeglumine (Berlex Laboratories, Wayne, NJ) (0.1 mmol/kg) was administered as a slow intravenous injection, and the T1-weighted SE sequence was then repeated. A 3DFT (volume) radiofrequency spoiled GRASS GRE sequence (10) was then performed with T1-weighted imaging parameters including 38/5, 45° flip angle, 64 partitions, and one signal average.

SE sequences were acquired with a 5-mm section thickness and a 1-mm intersection gap, whereas the volume spoiled GRASS sequence was performed with contiguous 2.0-mm sections. All pulse sequences were performed with an imaging matrix consisting of 192 (phase) × 256 (frequency) steps, 20-cm field of view, and spatial presaturation pulses applied inferior to the imaging volume. The phase direction was oriented along the right-to-left axis of the head for both sequences. Gradient moment nulling (flow compensation) was not used with either the SE or GRE T1-weighted sequences. Image acquisition time was 6 minutes 28 seconds for 2DFT SE and 7 minutes 48 seconds for 3DFT GRE pulse sequences. Window and level settings were optimized separately for SE and GRE images.

Intracranial lesions that demonstrated evidence of contrast enhancement on T1-weighted SE images were observed in 61

patients (15%). These patients (29 men, 34 women; age range, 24–87 years; mean, 61 years) formed the population for this study. A maximum of five lesions per patient was analyzed to avoid biasing of the results. A total of 101 enhancing intracranial lesions were analyzed, including 76 intraaxial and 25 extraaxial lesions. The number of lesions per patient was one ($n = 44$; 72%), two ($n = 7$; 11%), three ($n = 3$; 5%), four ($n = 1$; 2%), and five ($n = 6$; 10%). Pathologic classification of the lesions revealed that there were 68 neoplastic lesions, 13 infectious or inflammatory lesions, 11 ischemic lesions, and nine vascular lesions. The specific diagnoses are listed in the Table.

Quantitative determination of lesion enhancement, as displayed on 2DFT SE and 3DFT GRE images, was performed. An electronic region-of-interest cursor was used to measure signal intensity within the enhancing portion of each lesion. In addition, signal intensity measurements were obtained of apparently normal brain parenchyma adjacent to each lesion and of background noise measured outside of the patient in the phase-encoding direction of the image. A single measurement of each region was acquired. Cursor size, configuration, and position were chosen to encompass a large portion of the enhancing component of each lesion, and these parameters were kept constant for measurements obtained from 2DFT SE and 3DFT GRE images. From these measurements, calculation of the contrast-to-noise ratio (C/N) for each lesion was performed as follows: C/N = (SI lesion − SI brain)/(SD SI noise), where SI = signal intensity and SD = standard deviation (11). Statistical analysis of C/N measurements was performed with analysis of variance (ANOVA) and matched-pair t tests.

Qualitative comparison of relative conspicuity of lesion enhancement as displayed on 2DFT SE and 3DFT GRE images was also performed. A five-point scale was used to subjectively compare lesion enhancement. The enhancement of each lesion was graded as substantially greater on 2DFT SE images, slightly greater on 2DFT SE images, equivalent on 2DFT SE and 3DFT GRE images, slightly greater on 3DFT GRE images, or substantially greater on 3DFT GRE images. The pattern of lesion enhancement and factors relating to general image quality were also subjectively analyzed.

Quantitative and qualitative evaluations were performed by the same investigator. Qualitative review was performed in an unblinded manner with respect to sequence type, due to obvious differences between the two sequences.

RESULTS

Quantitative Results

The mean C/N for all lesions on 2DFT SE images was 17.6, with a standard deviation of 14.7. The mean C/N for all lesions on 3DFT GRE images
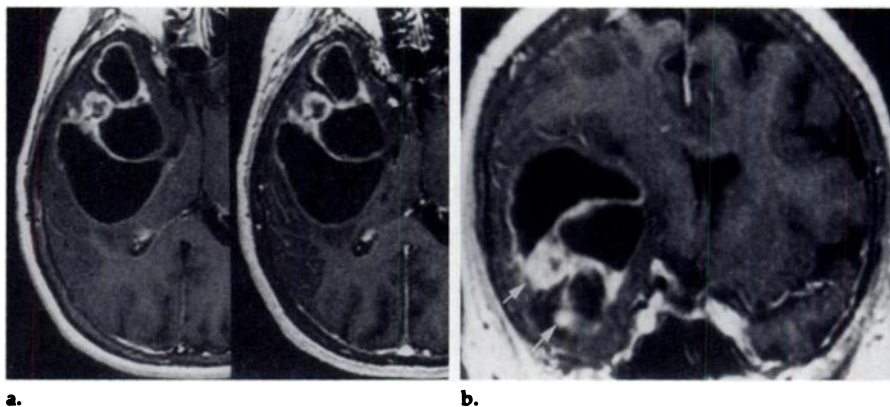

a.   b.

Figure 1. (a) Gadolinium-enhanced T1-weighted 2DFT SE (left) and 3DFT GRE (right) images obtained in a 72-year-old woman with glioblastoma involving the right temporal lobe show that contrast enhancement of multiple septa traversing the lesion is of equivalent conspicuity with both sequences. (b) The presence of nodular contrast-enhancing foci along the septal walls (arrows) is depicted on this coronal 3DFT GRE reformation, which also demonstrates mass effect on the ventricular system.

was 17.2, with a standard deviation of 15.9. There was no statistically significant difference between these C/N values, as determined by the matched-pairs t test ($P = .72$). Lesion C/N varied with the two sequences by 0%–50% (52 lesions), 51%–100% (20 lesions), 101%–200% (20 lesions), and greater than 200% (nine lesions).

The ratio of C/N for 2DFT SE to the C/N for 3DFT GRE imaging was calculated. The mean C/N ratio was 0.95 for extraaxial lesions and 1.17 for intraaxial lesions. There was no significant difference between these values ($P = .23$) by using the ANOVA test. C/N ratios were also analyzed according to type of lesion. The mean C/N ratios for neoplastic, inflammatory, vascular, and ischemic lesions were 1.26, 0.96, 0.96, and 0.57, respectively. Therefore, 2DFT SE images displayed somewhat greater C/N for neoplastic lesions, whereas 3DFT GRE images had greater C/N for ischemic lesions. Application of the Tukey method for pairwise comparison demonstrated a significant difference between the C/N ratios for neoplastic versus ischemic lesions but not for all other comparisons among these categories.

Qualitative Results

The relative conspicuity of lesion enhancement was qualitatively equivalent for 87 lesions (86.8%) (Fig 1). Enhancement was of mild relative increased conspicuity for five lesions (4.9%) on 2DFT SE images and for eight lesions (7.9%) on 3DFT GRE images (Fig 2). One lesion (0.9%) demonstrated marked relative increased enhancement on 3DFT GRE images. The types of lesions for which en-

Classification of Lesions

Type of Lesion	No. of Patients	No. of Lesions
Metastatic tumor	13	45
Subacute infarct	11	11
Meningioma	9	9
Venous angioma	5	5
Meningeal carcinomatosis	2	5
Glioma	4	4
Postoperative meningeal enhancement	4	4
Inflammatory*	2	3
Multiple sclerosis	1	3
Toxoplasmosis	1	2
Acoustic neuroma	2	2
Lymphoma	1	2
Cavernous angioma	2	2
Aneurysm	2	2
Ependymoma	1	1
Subdural hematoma†	1	1
Total	61	101

* Precise diagnosis not established.
† Enhancement present within surrounding membrane.

hancement was more conspicuous on 2DFT SE images included meningioma ($n = 3$) and metastases ($n = 2$). Those lesions for which enhancement was more conspicuous on 3DFT GRE images included acoustic schwannoma ($n = 2$), aneurysms ($n = 2$), meningioma ($n = 1$), metastasis ($n = 1$), subacute infarct ($n = 1$), postcraniotomy meningeal enhancement ($n = 1$), and vascular malformation ($n = 1$).

The pattern of contrast enhancement displayed by both types of images was similar in all patients. Small amounts of hemorrhage, however, were depicted with greater conspicuity on 3DFT GRE images in seven lesions (Fig 3). Hemorrhage was due to
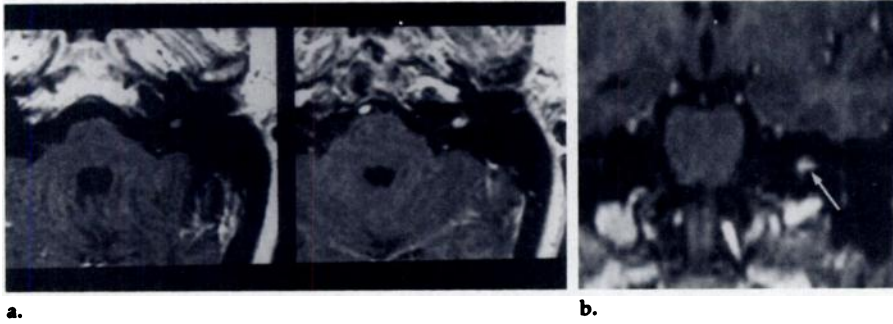
a.   **b.**

Figure 2. **(a)** Gadolinium-enhanced T1-weighted 2DFT SE (left) and 3DFT GRE (right) images obtained in a 55-year-old woman with small left intracanalicular acoustic schwannoma. The 3DFT GRE sequence results in more conspicuous enhancement of this lesion. **(b)** 3DFT GRE coronal reformation also displays the anatomic location of the lesion (arrow).
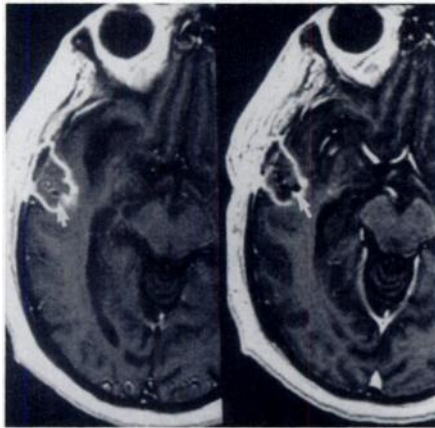

Figure 3. Gadolinium-enhanced T1-weighted 2DFT SE (left) and 3DFT GRE (right) images obtained in a 65-year-old man who recently underwent cerebral biopsy for suspected encephalitis show that conspicuity of contrast enhancement is equivalent on both images. Small foci of signal void representing hemorrhage (arrow) are more prominently displayed on the 3DFT GRE image but do not obscure visualization of lesion enhancement.

previous surgical intervention in three lesions and to hemorrhagic vascular malformation, subdural hematoma, hemorrhagic tumor, and hemorrhagic infarction in one lesion each. The presence of hemorrhage in these cases was depicted as foci of markedly decreased signal intensity in or adjacent to the described lesions. This area of signal loss did not substantially obscure visualization of enhancement of any lesion. Enhancement patterns varied slightly on 2DFT SE and 3DFT GRE images for four lesions in which decreased intensity of central lesion enhancement was more perceptible with the 3DFT GRE technique. Enhancement within the periphery of these lesions was similar on both sets of images. The 3DFT GRE images appeared to demonstrate greater detail regarding the internal structure of these lesions, which in-

cluded three metastases and one meningioma (Fig 4). Decreased differentiation of tumor margins from adjacent vascular structures was observed with 3DFT GRE images in two patients.

Excellent image quality was present for both pulse sequences in nearly all patients. Noticeably greater motion artifacts, however, were evident on 3DFT GRE images in six patients. 3DFT GRE images provided improved differentiation between gray and white matter, as well as decreased vascular pulsation artifacts within the posterior fossa (Fig 5).

DISCUSSION

3DFT GRE imaging offers many important advantages over conventional 2DFT SE imaging. One such advantage is improvement in spatial resolution (2). With the use of 3DFT GRE sequences, section thickness can be decreased beyond that which is available with 2DFT SE pulse sequences. In this study, I compared 2DFT SE images acquired by using a standard 5-mm section thickness with 3DFT GRE images acquired by using a 2-mm section thickness. With these parameters, voxel sizes for 2DFT SE images were 4 mm³, and those for 3DFT GRE images were 1.6 mm³. Voxel volume is inversely proportional to spatial resolution, which was 250% greater for 3DFT GRE than for 2DFT SE images. The minimum section thickness available for acquisition of 2DFT SE images with our system is 3 mm. While improved spatial resolution could have been achieved in 2DFT SE imaging with 3-mm-thick sections, this would have resulted in prolonged examination time to provide coverage of the entire brain and decreased signal-to-noise ratio (S/N). The objective of this study was to evaluate the ability of 3DFT GRE im-

aging to serve as a practical alternative to routine contrast-enhanced T1-weighted 2DFT SE imaging. The study was also designed to evaluate pulse sequences that involved comparable imaging times.

In addition to providing markedly reduced voxel volumes, the use of 3DFT GRE imaging also results in the elimination of intersection gaps. Such gaps are used in 2D imaging to minimize the reduction in S/N and T1 contrast, which occur due to cross excitation resulting from imperfect section excitation profiles (12–14).

The 3DFT GRE sequence used had a slightly greater acquisition time (1.3 minutes) than did the 2DFT SE sequence. Image acquisition time is determined for 2DFT sequences by the product of TR, number of signal averages, and number of phase-encoding steps. For determination of image acquisition time in 3DFT sequences, this figure must be multiplied by the number of phase-encoding steps performed in the section-select direction (also known as partitions). It is this additional factor that renders performance of 3DFT SE imaging impractical because of excessive acquisition time. With GRE imaging, however, the TR can be markedly reduced while maintaining adequate S/N and T1 contrast. Further reduction in acquisition times for volume GRE sequences may be achieved in the future by using techniques such as magnetization prepared rapid acquisition GRE (15).

The excitation of a large volume of tissue rather than individual sections leads to another important advantage for 3DFT GRE imaging. 3DFT GRE images may be reformatted in any orthogonal or oblique imaging plane after images have been acquired and the patient has left the department (2). Such reformations may also be acquired along a tilted or curved plane and can be generated in near real time by using current image-processing workstations. Since in many centers the plane in which postcontrast T1-weighted images are acquired is varied according to the suspected location of the abnormality (ie, coronal imaging for internal auditory canals and temporal lobes, sagittal imaging for parasellar region), the ability to perform high-quality multiplanar reconstructions of a previously acquired data set allows for simplification of imaging protocols. Time savings may also be achieved, since multiple different enhanced T1-weighted sequences do not have to be acquired.

When isotropic 3D imaging is performed (2), the spatial resolution of the reconstructed images is equivalent to that present in the plane of image acquisition (ie, transaxial plane in this study) (2). This implies that the three cubic dimensions of the voxel are equal. In our series, an anisotropic 3D data set was acquired, since voxel dimensions measured 1.0 × 0.8 × 2.0 mm. Despite the relatively mild degree of anisotropy that was present, multiplanar reformations were obtained in all of our patients by using an image-processing workstation and were usually qualitatively equivalent in image quality to the original transaxial images. These reformations were highly valuable for demonstration of many anatomic and pathologic features that were less optimally visualized in the transaxial imaging plane (16) (Figs 1, 2, 4–6).

The sensitivity of 3DFT GRE imaging to depiction of flow-related phenomena is often advantageous. Vascular lesions such as aneurysms and vascular malformations, as well as prominent vascularity related to ischemic or neoplastic processes, are displayed with marked intensity on 3DFT GRE images (17,18) (Fig 6). Vascular structures and lesions may be poorly depicted on enhanced 2DFT SE images. This is due to the counterbalancing effects of intraluminal signal loss from spin phase and time-of-flight flow phenomena (19) and intraluminal enhancement resulting from the T1 shortening effects of gadopentetate dimeglumine. The relative prominence of these effects varies according to the type of flow that predominates. Signal loss often occurs when there is rapid and/or turbulent flow, whereas with slow laminar flow, this effect is often overwhelmed with contrast enhancement. Combinations of these patterns are observed in some vascular lesions, and the coexistence of these effects may lead to isointensity of the vessel relative to surrounding structures.

The 3DFT GRE technique forms the basis for one of the more commonly performed methods of MR angiography (20–24). Cerebral MR angiograms can, in fact, be displayed from the data set we acquired after processing through a maximum-intensity projection software algorithm. The imaging parameters used in this study, however, were optimized for depiction of enhancing lesions rather than for use with MR angiography. Anatomic information regarding vascular lesions was better displayed on multiplanar reformations of the 3DFT GRE data
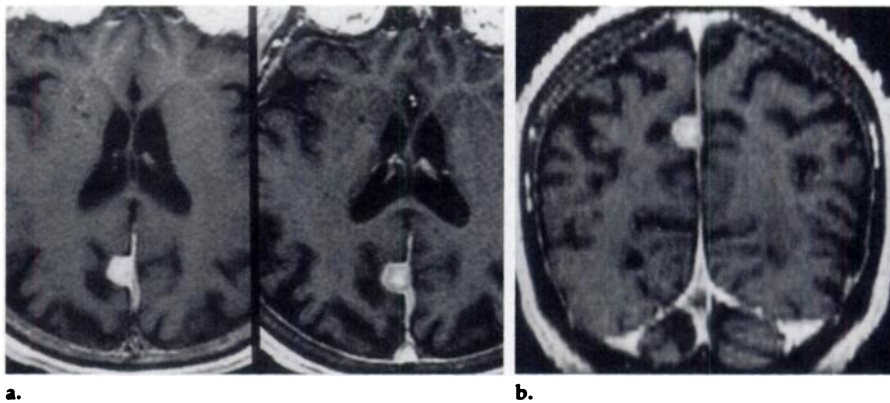

Figure 4. Contrast-enhancing meningioma based along the posterior falx cerebri in an 84-year-old man. (a) Lesion enhancement is well demonstrated on both 2DFT SE (left) and 3DFT GRE (right) images. The 3DFT GRE image appears to demonstrate more detail regarding the internal structure of the lesion on both the original transaxial and (b) the reformatted coronal displays.
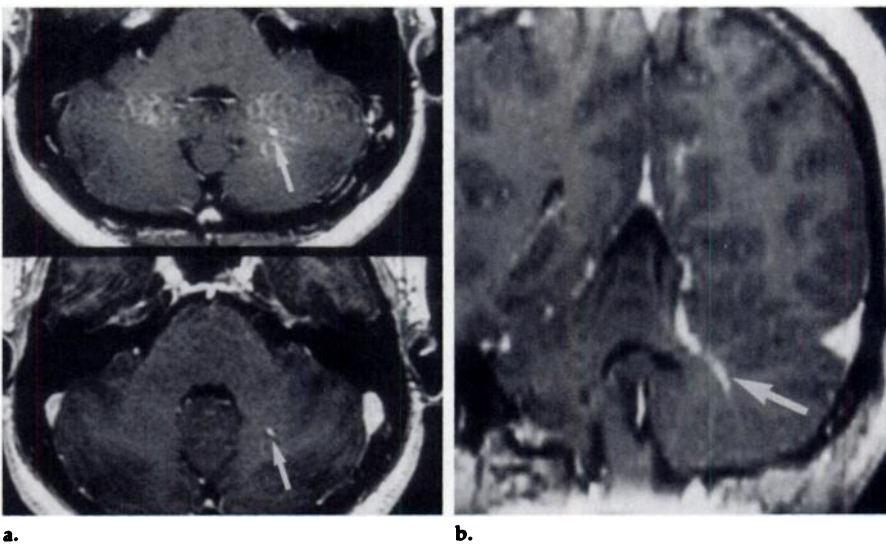

Figure 5. (a) Decreased vascular pulsation artifact within the posterior fossa is present on 3DFT GRE (bottom) and 2DFT SE (top) gadolinium-enhanced images. A small focus of enhancement (arrows) within the left cerebellar hemisphere is present on both images obtained in a 32-year-old woman. (b) The tubular nature of this presumed venous angioma (arrow) and its extension to the tentorium cerebelli are better appreciated on this coronal oblique 3DFT GRE reformation.

set than on MR angiograms acquired with the maximum-intensity projection process.

Flow-related artifacts are accentuated on 2DFT SE images that are acquired after administration of gadopentetate dimeglumine due to the intraluminal T1-shortening effects of the contrast agent (25). The prominence of such artifacts, which are usually most severe in the posterior fossa adjacent to the venous sinuses, may be decreased with use of spatial presaturation. Gradient moment nulling (flow compensation) techniques may also reduce flow artifacts but cannot be implemented with short TE SE imaging. The shorter TEs available with 3DFT GRE imaging, as well as the reduced section thickness, however,

lead to a further reduction of flow artifacts (Fig 5). Increased intraluminal signal intensity on 3DFT GRE images may occasionally have the undesirable effect of decreasing visualization of vascular structures that are surrounded by an enhancing lesion.

Demonstration of hemorrhagic breakdown products was improved on 3DFT GRE images as compared with that on 2DFT SE images. The presence of deoxyhemoglobin within acute hematomas or hemosiderin related to chronic hematomas is usually poorly visualized on T1-weighted SE images (26). However, GRE images are more sensitive to local fluctuations in magnetic field gradient (ie, susceptibility effects) than are SE images, due to the absence of a 180° refocus-
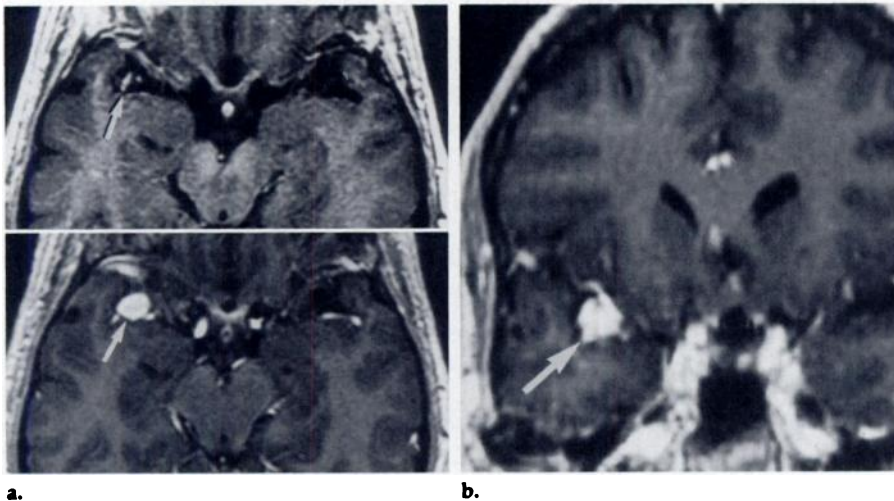
a.   **b.**

Figure 6. Right middle cerebral artery aneurysm in a 38-year-old man. (a) Contrast-enhanced 3DFT GRE image (bottom) displays considerably more intense and homogeneous enhancement throughout the lesion (arrow) than does the corresponding 2DFT SE image (top). (b) The anatomic location of the lesion (arrow) and its relationship to adjacent vessels are well visualized on this 3DFT GRE coronal reformation.

ing pulse (27,28). On GRE images, these hemorrhagic products (as well as calcifications) (29) are depicted as foci of markedly reduced signal intensity (Fig 3). The hypointensity caused by hemorrhagic foci did not obscure visualization of surrounding lesion enhancement in any of the patients in this series. Susceptibility effects may potentially result in artifacts on GRE images at interfaces between soft tissue and bone or air (30). Such susceptibility artifacts, however, were minor on 3DFT GRE images in our study, due to the very short TE and 3DFT that were used (31). The accentuation of susceptibility effects on 3DFT GRE images may result in degradation of image quality within the extracranial soft tissues.

3DFT GRE and 2DFT SE images displayed nearly identical patterns of contrast enhancement in most lesions. There were several lesions, however, in which 3DFT GRE images appeared to result in more detailed depiction of internal lesion architecture (Fig 4). This finding is also likely due to susceptibility effects, with the areas of relatively decreased signal intensity caused by hemorrhagic, calcific, or perhaps less cellular lesion components. It is possible that demonstration of such features could contribute to lesion characterization, and this issue deserves further study. It is possible, though unlikely, that the observed differences in patterns of contrast enhancement on 3DFT GRE versus 2DFT SE images could be related in part to temporal changes, since 3DFT GRE images were acquired after 2DFT SE images. The ef-

fect of such temporal factors relating to conspicuity of lesion enhancement also cannot be completely ruled out.

The occurrence of patient motion during image acquisition leads to more severe artifacts on 3DFT GRE images than on 2DFT SE images. Such artifacts may result in image blurring or in replications of anatomic structures, both of which obscure anatomic detail (32). 3DFT GRE images are more sensitive to motion because phase encoding is performed in two axes rather than one. This factor may limit the usefulness of 3DFT GRE imaging in uncooperative patients, though in this series, substantially increased motion artifacts on 3DFT GRE images were present in only six patients. It should also be noted that 3DFT GRE images were acquired after 2DFT SE images in all patients in this study, which might contribute to greater patient motion on 3DFT GRE images.

3DFT GRE imaging may also result in reduced S/N as compared with 2DFT SE images. S/N is directly proportional to TR, flip angle, number of signals averaged, and number of partitions, whereas it is inversely proportional to TE (33). Calculation of relative S/N for these sequences indicates that 2DFT SE images were of approximately four times greater S/N than were 3DFT GRE images. There are additional factors that may alter S/N, such as cross excitation between adjacent imaging sections and the effects of artifacts due to motion, susceptibility, chemical shift, and others. While this relative reduction in S/N on 3DFT GRE images was noticeable, it did not result in substantial image

graininess or in decreased lesion conspicuity.

The above discussion indicates that while 3DFT GRE imaging presents some relative limitations, there are many more important advantages it offers over conventional 2DFT SE imaging. However, if 3DFT GRE imaging is to serve as a substitute for 2DFT SE T1-weighted sequences in the clinical setting, it must be established that sensitivity to depiction of contrast enhancement within intracranial lesions is not being sacrificed. This study indicates that lesion enhancement on 3DFT GRE images is quantitatively and qualitatively equivalent to that depicted on 2DFT SE images.

Because 3DFT GRE imaging was performed only after administration of contrast material, the value of unenhanced 3DFT GRE imaging cannot be addressed. In addition, this study did not determine the sensitivity or specificity of 2DFT SE versus 3DFT GRE imaging for lesion detection. To do so would require absolute proof of the presence or absence of all lesions, which could only be obtained with correlative postmortem examinations.

In conclusion, 3DFT GRE imaging offers many important advantages over conventional 2DFT SE imaging. Contrast enhancement of intracranial lesions was depicted on 3DFT GRE images with conspicuity equivalent to that on 2DFT SE images. These findings indicate that 3DFT GRE pulse sequences are likely to play a major role in the performance of contrast-enhanced MR imaging of the brain. ∎

References
1. Frahm J, Haase A, Matthaei D. Rapid three-dimensional MR imaging using the FLASH technique. J Comput Assist Tomogr 1986; 10:363–368.
2. Runge VM, Wood ML, Kaufman DM, Nelson KL, Traill MR. FLASH: clinical three-dimensional magnetic resonance imaging. RadioGraphics 1988; 8:947–965.
3. Hesselink JR, Healy ME, Press GA, Brahme FJ. Benefits of Gd-DTPA for MR imaging of intracranial abnormalities. J Comput Assist Tomogr 1988; 12:266–274.
4. Elster AD, Moody DM, Ball MR, Laster DW. Is Gd-DTPA required for routine cranial MR imaging? Radiology 1989; 173: 231–238.
5. Runge VM, Carollo BR, Wolf CR, Nelson KL, Gelblum DY. Gd DTPA: a review of clinical indications in central nervous system magnetic resonance imaging. RadioGraphics 1989; 9:929–958.
6. Kucharczyk W, Lee DH, McClarty B, Robertson WD, Hele MJ. Routine contrast enhancement for cranial magnetic resonance imaging: an analysis of its diagnostic value in adults. Can Assoc Radiol J 1991; 42:199–209.
7. Ross JS, Masaryk TJ, Modic MT. Three-dimensional FLASH imaging: applications

with gadolinium-DTPA. J Comput Assist Tomogr 1989; 13:547–552.

8. Schörner W, Sander B, Henkes H, Heim T, Lanksch W, Felix R. Multiple slice FLASH imaging: an improved pulse sequence for contrast enhanced MR brain studies. Neuroradiology 1990; 32:474–480.

9. Cherryman G, Golfieri R. Comparison of spin echo T1-weighted and FLASH 90° gadolinium-enhanced magnetic resonance imaging in the detection of cerebral metastases. Br J Radiol 1990; 63:712–715.

10. Wang HZ, Riederer SJ. Spoiling sequence for suppression of residual transverse magnetization. Magn Reson Med 1990; 15:175–191.

11. Kaufman L, Kramer DM, Crooks LE, Ortendahl DA. Measuring signal-to-noise ratios in MR imaging. Radiology 1989; 173:265–267.

12. Bradley WG, Glenn BJ. Effect of variation in slice thickness and interslice gap on MR lesion detection. AJNR 1987; 8:1057–1062.

13. Kucharczyk W, Crawley AP, Kelly WM, Henkelman RM. Effect of multislice interference on image contrast in T2- and T1-weighted MR images. AJNR 1988; 9:443–451.

14. Schwaighofer BW, Yu KK, Mattrey RF. Diagnostic significance of interslice gap and imaging volume in body MR imaging. AJR 1989; 153:629–632.

15. Runge VM, Kirsch JE, Thomas GS, Mugler JP III. Clinical comparison of three-dimensional MP-RAGE and FLASH techniques for MR imaging of the head. JMRI 1991; 1:493–500.

16. Wood ML, Runge VM. Application of image enhancement techniques to magnetic resonance imaging. RadioGraphics 1988; 8:771–784.

17. Needell WM, Maravilla KR. MR flow imaging in vascular malformations using gradient recalled acquisition. AJNR 1988; 9:637–642.

18. Atlas SW, Mark AS, Fram EK, Grossman RI. Vascular intracranial lesions: applications of gradient-echo MR imaging. Radiology 1988; 169:455–461.

19. Bradley WG Jr. Carmen lecture: flow phenomena in MR imaging. AJR 1988; 150:983–984.

20. Ruggieri PM, Laub GA, Masaryk TJ, Modic MT. Intracranial circulation: pulse-sequence considerations in three-dimensional (volume) MR angiography. Radiology 1989; 171:785–791.

21. Marchal G, Bosmans H, Van Fraeyenhoven L, et al. Intracranial vascular lesions: optimization and clinical evaluation of three-dimensional time-of-flight MR angiography. Radiology 1990; 175:443–448.

22. Masaryk TJ, Modic MT, Ross JS, et al. Intracranial circulation: preliminary clinical results with three-dimensional (volume) MR angiography. Radiology 1989; 171:793–799.

23. Masaryk TJ, Modic MT, Ruggieri PM, et al. Three-dimensional (volume) gradient-echo imaging of the carotid bifurcation: preliminary clinical experience. Radiology 1989; 171:801–806.

24. Sevick RJ, Tsuruda JS, Schamalbrock P. Three-dimensional time-of-flight MR angiography in the evaluation of cerebral aneurysms. J Comput Assist Tomogr 1990; 14:874–881.

25. Richardson DN, Elster AD, Williams DW III. Gd-DTPA–enhanced MR images: accentuation of vascular pulsation artifacts and correction by using gradient-moment nulling (MAST). AJNR 1990; 11:209–210.

26. Gomori JM, Grossman RI. Mechanisms responsible for the MR appearance and evolution of intracranial hemorrhage. RadioGraphics 1988; 8:427–440.

27. Atlas SW, Mark AS, Grossman RI, Gomori JM. Intracranial hemorrhage: gradient-echo MR imaging at 1.5 T—comparison with spin-echo imaging and clinical applications. Radiology 1988; 168:803–807.

28. Seidenwurm D, Meng TK, Kowalski H, Weinreb JC, Kricheff II. Intracranial hemorrhagic lesions: evaluation with spin-echo and gradient-refocused MR imaging at 0.5 and 1.5 T. Radiology 1989; 172:189–194.

29. Atlas SW, Grossman RI, Hackney DB, et al. Calcified intracranial lesions: detection with gradient-echo-acquisition rapid MR imaging. AJR 1988; 150:1383–1389.

30. Winkler ML, Ortendahl DA, Mills TC, et al. Characteristics of partial flip angle and gradient reversal MR imaging. Radiology 1988; 166:17–26.

31. Haacke EM, Tkach JA, Parrish TB. Reduction of T2* dephasing in gradient field-echo imaging. Radiology 1989; 170:457–462.

32. Hinks RS, Quencer RM. Motion artifacts in brain and spine MR. Radiol Clin North Am 1988; 26:737–753.

33. Carlson J, Crooks LE, Ortendahl DA, Kramer DM, Kaufman L. Signal-to-noise ratio and section thickness in two-dimensional versus three-dimensional Fourier transform MR imaging. Radiology 1988; 166:266–270.